*International Journal for Modern Trends in Science and Technology*
*Volume 12, Issue 04*, pages 292-298.
ISSN: 2455-3778 online
Available online at: http://www.ijmtst.com/vol12issue04.html
DOI: https://doi.org/10.5281/zenodo.19441069

# A Single-Stage Bridgeless PFC Charger With Enhanced Power Quality for LEV-Mounted Solar PV Panel

**M. Giri Babu, J. Prashanth, T. Kavya, A.Srujan, K. Isaac Babu, P. Sireesha**

*Department of Electrical and Electronics Engineering, PBR Visvodaya Institute of Technology and Science, Kavali, India.*

**To Cite this Article**
M. Giri Babu, J. Prashanth, T. Kavya, A.Srujan, K. Isaac Babu & P. Sireesha (2026). A Single-Stage Bridgeless PFC Charger With Enhanced Power Quality for LEV-Mounted Solar PV Panel. International Journal for Modern Trends in Science and Technology, 12(04), 292-298. https://doi.org/10.5281/zenodo.19441069

**Article Info**
Received: 06 March 2026; Revised: 28 March 2026; Accepted: 01 April 2026.



***KEYWORDS***

*Light electric vehicle (LEV), maximum power point tracking (MPPT), power factor-corrected (PFC) charger, solar photovoltaic (PV), total harmonic distortion (THD)*

**ABSTRACT**

*Growing popularity of electric vehicles (EVs) along with solar photovoltaic (PV) has inspired researchers to com- bine both segments for sustainable future growth. A light EV (LEV)-mounted PV panel is one such expanding sector. However, very little literature is on onboard charging solutions that have interfaced both grid and solar PV inputs for an LEV-mounted PV panel, leaving room for improvisation. Power factor-corrected (PFC) charger presented in this article focuses on the same and interfaces with grid, PV panel, and battery to form a three-port topology. Both grid and PV panel can charge battery independently as well as in synchrony. It aims to improve the total harmonic distortion (THD) of source current in compliance with the IEC 61000-3-2 standard and reduce the total number of components. Small-signal modeling along with ac-sweep analysis in PSIM software is employed for controller design for each input. A variable step-size maximum power point tracking (MPPT) technique provides perturbation-free output from PV panel in steady state. It is intended to operate optimally even in dynamically challenging situations, including sudden changes in grid voltage, broad variations in output power demand, and unexpected disruption in one of the power inputs. Operation of charger is demonstrated by developing a laboratory prototype operating at 500 W output power and yielding 1.2% THD in grid current.*

## INTRODUCTION

The growing acceptability and appeal of light electric vehicles (LEVs) with a photovoltaic (PV) panel installed atop the vehicle, particularly in developing nations such as India, has opened up new research avenues. One of the most active research areas is electric vehicle (EV) charging systems. Over the past decades, multiple power factor-corrected (PFC) chargers have been

proposed for fully grid-dependent EVs Notably, these configurations are classed as single-stage two-stage charger based on their architecture. Core premise of a PFC charger is to supply a ripple-free current to battery while also maintaining a high-power factor at the input. Two-stage topologies need two converters (ac–dc and dc–dc) to accomplish both functions. However, a single ac–dc interfacing converter carries out both functions in single-stage charging. Henceforth, it has an intrinsic benefit of a simpler structure and improved efficiency Galvanic isolation is generally employed in a two-stage onboard charger by incorporating an isolated dc–dc converter in second stage. However, SAE J1772 standard does not necessitate the employment of transformers as a safety requirement for EVs. Additionally, battery ground is always in a floating state with the chassis of a vehicle, so it is not necessary to provide isolation with grid input ,Instead, compact and cost-effective relay circuits can replace the bulky transformer for safety measures in addition, incorporation of transformers in isolated topologies increases size, losses, complexities, and switch stress due to leakage inductance. Hence, no isolated single-stage topologies are becoming popular as cost-effective charging solutions for LEVs.

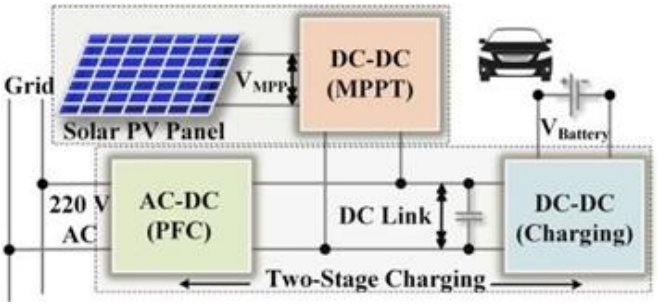


FIG 1.Conventional solar PV incorporated PFC charging system.

Generally, boost converter-based PFC topology is very popular for sinusoid current shaping of grid input Nevertheless, its utilization for single-stage low-voltage charg- ing applications is limited due to output voltages higher than the peak of grid voltage. To address these issues, other topologies with buck-boost capabilities, such as Cuk, SEPIC, and Zeta are commendable options for such applications Among all aforementioned options, Cuk converter-derived topologies offer several benefits, including native protection against inrush current and providing continuous current at input and output.

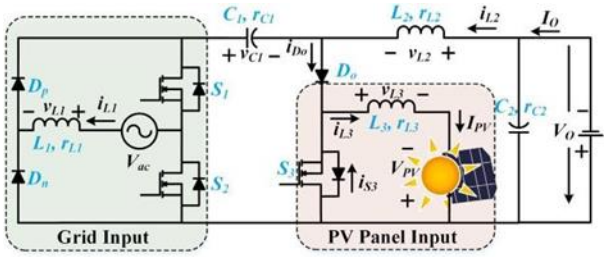


Fig. 2. Schematic of bridgeless LEV charger.

## STRUCTURE OF PAPER

The paper is organized as follows: A single-stage bridgeless PFC charger for an LEV-mounted solar PV panel consists of a solar PV input connected through an input filter to reduce EMI and ripple. The filtered power is fed into a bridgeless PFC converter, typically a boost-type configuration using active switches, diodes, and an inductor, eliminating the conventional diode bridge to reduce conduction losses and improve efficiency. This stage performs both power factor correction and DC-DC conversion in a single stage, ensuring near-unity power factor and low harmonic distortion.

The output is passed through a DC-link capacitor that stabilizes the voltage and filters switching ripples. The regulated DC power is then supplied to the battery charging unit, which operates under constant current and constant voltage modes suitable for LEV batteries. A control system, usually based on a microcontroller or DSP, manages switching through PWM techniques and incorporates MPPT to extract maximum power from the solar PV panel.

## OBJECTIVES

1. To design a single-stage bridgeless PFC charger for improved efficiency in LEV applications.
2. To enhance input power quality by reducing total harmonic distortion (THD).
3. To achieve a high-power factor close to unity.
4. To minimize conduction and switching losses using a bridgeless topology.
5. To integrate solar PV input for sustainable and renewable energy utilization.
6. To ensure continuous and reliable charging of Light Electric Vehicle (LEV) batteries.
7. To reduce input current distortion and improve waveform shaping.

8. To develop a compact and cost-effective charging solution.
9. To improve overall energy conversion efficiency of the charging system.
10. To comply with power quality standards for grid-connected systems..

## CONFIGURATION AND OPERATION PRINCIPLES

The bridgeless multiport PFC charger presented in this article inherits the merits of a typical Cuk PFC rectifier and fol- lows a similar operating principle. Furthermore, modification of a conventional two-port Cuk converter allows the addition of PV panel input. The modified topology presented here comprises three inductors and two capacitors and is shown in Fig. 2. In addition, it also necessitates the use of three diodes and three switches. Here, two diodes of DBR are replaced by two switches, namely S1 and S2, to create a bridgeless design for ac input. During positive voltage polarity, diode Dp conducts, while during negative voltage polarity, diode Dn conducts. The instantaneous sinusoidal grid voltage applied at primary input is denoted as Vac(t) = Vp sin(314t). (1)

In above equation, Vp represents peak value of Vac(t). Since switching frequency is relatively high in comparison with grid frequency, Vac(t) can be assumed constant and expressed as Vac in a single switching cycle. Similarly, time-varying duties DS1(t) and DS2(t) of grid input and PV input, respectively, can be represented as DS1 and DS2 in a switching period. Switches S1 and S2 are controlled by DS1. Meanwhile, switch S3 is operated by DS2 in tandem with other two switches to perform the MPPT of PV panel input. Charger operates in three charging states, namely dual input charging, grid charging,

A. Dual Input Charging

Dual input charging uses inputs from both grid and PV system to charge batteries. Three modes of operation are used to demonstrate the operation of the charger during a single switching cycle for grid-PV charging. The logic employed for generation of control pulses for each mode is depicted in Fig. Here, d1, d2, and d3 represent duration of modes 1, 2, and 3, respectively. Operation of charger for positive voltage polarity is shown in Fig. Likewise, Fig. demonstrates its operation for negative polarity. In mode 1 and mode 3, switches S1
and S2 conduct while S3 does so in mode-3.

B. Grid Charging

Grid charging of the suggested converter is equivalent to a conventional PFC Cuk charger and hence power transfer takes place in two modes of operation. Fig. 3(h) and (i) depicts the converter's functioning in modes 1 and 2, respectively. Switches S1 and S2 are turned on and off in mode 1 and mode 2, respectively, while conducting S3 in both modes. Additionally, inductors L1 and L2 are charged and C1 is discharged in mode 1. Similarly, in mode 2, L1 and L2 discharge while C1 charges.

C.PV Stand-Alone Charging

The presented converter has the ability to harness solar energy even while driving or parked by roadside. It is depicted in Fig. 3(j) and (k) and is known as PV stand-alone charging. PV panel transfers its energy to the output through an intermediate capacitor. However, it is only carried out in two modes of operation by switching S3 in each mode and conducting S1 and S2 all the time

TABLE I SYSTEM SPECIFICATIONS

| Specifications | Parameters | Value (Range) |
|---|---|---|
| AC Mains | Voltage ($V_{ac}$) | 110 V (90 V-130 V) |
| | Power ($P_{ac}$) | |
| PV Panel | Voltage at MPP ($V_{pv}$) | |
| | Power at MPP ($P_{pv}$) | |
| Output | Voltage ($V_o$) | |
| | Power ($P_o$) | 470 W ($P_{max}$ = 570 W) |
| Switching Freq. | | 20 kHz |

TABLE II EXPERIMENTAL COMPONENT RATING

| Device | Rating |
|---|---|
| Grid Input Inductor ($L_1$) | 6 mH, ESR($r_{L1}$)=0.26 Ohm |
| Output Inductor ($L_2$) | 1.5 mH, ESR($r_{L2}$)=0.13 Ohm |
| PV Input Inductor ($L_3$) | 4.8 mH, ESR($r_{L3}$)=0.2 Ohm |
| Intermediate Capacitor ($C_1$) | 5 $\mu$F |
| DC Link Capacitor ($C_2$) | 5.6 mF |

## SYSTEM DESIGN

DESIGN OF LEV CHARGER

This section provides detailed design equations of the presented charger. Based on system specifications provided in Table I, charger is designed to operate in continuous conduction mode (CCM). Output voltage of the charger ranges from 63 (Vo,min) to 87 V (Vomax),

where a lower voltage indicates a fully discharged state of battery and a higher voltage indicates a fully charged state. Output power of charger varies greatly and almost linearly with the output voltage. It is intended to handle an abrupt sag [down to 90 V (Vac,min)] and swell [up to 130 V (Vac,max)] in grid voltage. As a result, for all essential operating circumstances [(Vac,min, Vo,min), (Vac,min, Vo,max), (Vac,max, Vo,min), (Vac,max, Vo,max)], each inductor and capacitor should be designed to work in CCM

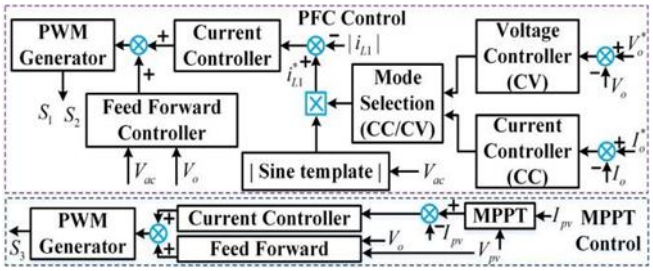


**SOLAR PHOTOVOLTAIC SYSTEM**

A typical solar PV system consists of several components including solar panels, a DC-DC converter, maximum power point tracking (MPPT) controller, inverter, and grid connection.

The DC power generated by the PV system is converted into alternating current (AC) using an inverter so that it can be integrated with the power grid.

Solar PV systems offer several advantages such as low maintenance, long operating life, and environmentally friendly power generation. Due to these benefits, solar PV systems are widely used in modern power systems.

Table: Line Data of the IEEE 14 Bus System Fig: Solar PV energy system

| Name of the module | Parameter values |
|---|---|
| PV array | Vmp=54.7V, Imp=5.58A, Voc=64.2V, Isc=5.96A,Ns=40,Np=820, pv=10MW. |
| Boost converter | Lb=5mH, Cin=100uF,Rdiode=0.1Ω, Rigbt=0.05Ω, Cout=12000uF. |

**MODELING AND CONTROL OF LEV CHARGER**

1. System Modeling

The model typically represents the hardware stages of the charger. For a DC Fast Charger (Level 3), the system is modeled in two main stages:

AC/DC Rectification (Front-end): An Active Front End (AFE) converter (usually a PWM rectifier) converts grid AC to a stable DC bus. The model must account for Power Factor Correction (PFC) to ensure the charger doesn't "pollute" the grid with harmonics.

DC/DC Conversion (Back-end): An isolated DC/DC converter (like an LLC resonant converter or Phase-Shifted Full Bridge) steps the DC bus voltage up or down to match the battery's real-time requirements.

The Load (Battery): The battery is modeled as a massive capacitor in series with internal resistance (R_{int}), where the voltage (V_{batt}) increases as the State of Charge (SoC) rises.

2. Control Strategies

The control system must be "battery-centric," adapting to the chemical limits of the cells.

Constant Current (CC) Control: During the initial stage (low SoC), the controller regulates the DC/DC converter to provide a steady, maximum allowable current.

Constant Voltage (CV) Control: Once the battery reaches its upper voltage limit (usually around 80% charge), the controller switches to maintaining a precise voltage, letting the current naturally taper off to prevent overcharging.

5 by * shape. Through- out the frequency range, it completely overlaps the plant Bode plot produced from preceding discussion. The designed controller (Gc) along with corresponding loop-gain is also shown in Fig. 5. A proportional and integral (PI) compensator for PFC control is employed here for the outer loop. Its primary objective is to track the battery current reference. Its bandwidth is kept low to limit the impact of low-frequency output current ripple on grid current. The outer current compensator of PFC control generates a current reference

that is further multiplied by a rectified unit sine template to generate i ∗ 1. An absolute value of the proposed approach can be extended to larger power systems and validated using real-time simulation platforms.

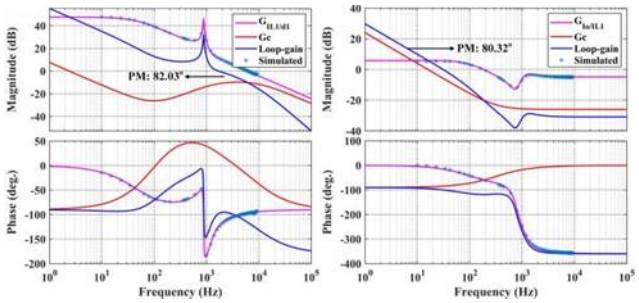


Fig. 5. Frequency response of (a) GIL1/d1, controller (type-3) and loop-gain, and (b) GIo/IL1, controller (PI) and loop-gain.

The generalized state equation is written as

$x^{\cdot} = [A_j][x] + [B_j][u]$ and $y = [C_j][x] + [D_j][u]$. (10)

In this context[, ] x = [ iL1, iL2, iL3, vC1, vC]2 T ,[ ] y = [ iL1, iL3, ]io T ,[ ]u = [ Vac, Vbat, ] VPV T . Appendix contains matrices for each mode of operation in the equation above. It is followed by averaging and the average state space equation is shown as

$\bar{x}^{\cdot} = [A_{avg}][x] + [B_{avg}][u]$ and

$\bar{y} = [C_{avg}][x] + [D_{avg}][u]$

sensed inductor current (iL1) is compared with generated reference $i * 1$ and passed to the inner current controller.

A type-3 compensator is employed for inner loop control to provide an adequate phase margin. The bandwidth of inner loop is comparatively high for faster dynamics and effective PFC control. As evident from frequency response of loop-gain in Fig. 5, phase margin of the inner and outer loop are 82.03◦ and 80.32◦, respectively. The result and discussion section further validates the controller's stable dynamic performance under diverse operating conditions.

## EFFICIENCY ANALYSIS AND COMPARISON

To perform the system efficiency analysis, a current stress calculation (rms and average) through each element is nec- essary. In a typical PFC charger operating in CCM, switch and diode currents are pulsewidth modulated and vary with time throughout the line cycle of grid input. Since switching frequency of the charger is much higher than grid frequency, a quasi-steady-state operation can be assumed for the rms and average current calculation Total rms current of each inductor (IL1,rms, IL2,rms, and IL3,rms) is obtained from its low- and high-frequency components. The average power loss over a line cycle is calculated for the hardware components given in Table and summarized in Table Here IS1,rms, IS2,rms, and IS3,rms are rms currents of switches S1, S2, and S3, respectively. The average from the linearized state space equation. Fig. 5 depicts the Bode plots of these plant transfer functions. To verify the small signal transfer functions, an ac-sweep of the presented topology from 10 Hz to 10 kHz is performed in PSIM and findings are indicated in Fig.

switches (S1 and S3) contribute to switching loss ( PS1,ON, PS1,OFF, and PS3,OFF), as third switch (S2) always conducts in an alternate voltage polarity. Switch S3 turn-off loss ( PS3,OFF) is the sole factor taken into account when calculating switching loss because it achieves the ZVS when turned on. The graphical distribution of loss component is shown in Fig.

Presented charger is compared with other reported topologies in terms of configuration and performance, and the same is summarized in Table. To diversify the analysis, comparison is performed with single input onboard charger, two stage dual input charger and single stage dual input integrated charger.

TABLE IV
COMPONENTS USED FOR LOSS ESTIMATION

| Device | Part-Number |
|---|---|
| MOSFET ($S_1 - S_3$) | NVHL040N120SC1 |
| Output Diode ($D_o$) | |
| Input Diode ($D_p$, $D_n$) | |
| Intermediate Capacitor ($C_1$) | |
| DC Link Capacitor ($C_2$) | |

THD in comparison with other solutions. To further justify the presented charger's performance, its THD at different loading is compared with topologies presented in and and is shown in Fig. THD in the grid current is quite low even at light loading in comparison with other solutions.

Unlike converters proposed in and the presented solution provides an additional solar PV interface with a reduced component count. Though work in and provide a multi-input and multifunctional topology, but it requires a large number of switching components, which

ultimately increases the size and cost of the charger. In contrast to multi-input integrated charger introduced in and presented charger can utilize both inputs simultaneously and independently. In addition, its bridgeless interface at grid input provides additional benefits over DBR-interfaced topologies inand Furthermore, unlike multi-input counterparts and presented charger reduces

**RESULT**

The implementation of a single-stage bridgeless PFC charger with enhanced power quality for a LEV-mounted solar PV panel yields the following results:

Improved Power Factor

The charger achieves a near-unity power factor (≈0.98–0.999), minimizing reactive power and improving overall energy utilization.

Reduced Harmonic Distortion

Total Harmonic Distortion (THD) of the input current is significantly reduced, complying with standards like IEC 61000-3-2, leading to cleaner grid interaction.

Higher Conversion Efficiency

Due to the bridgeless topology (elimination of diode bridge losses), efficiency is increased (typically >90–95%), reducing thermal stress and energy loss.

Enhanced Power Quality The system ensures:

Sinusoidal input current waveform Reduced voltage/current ripple Stable DC output for battery charging

Compact and Cost-Effective Design

Single-stage structure integrates PFC and DC-DC

| TYPESOF LOSSES | Expressions | Value |
|---|---|---|
| MOSFET Conduction | | |
| MOSFET Switching | $P_{Diode} = V_{Do}I_{Do,Avg} + I^2_{Do,RMS}r_I + V_{Dp}I_{Dp,Avg} + I^2_{Dp,RMS}r_I$ | |
| Diode Conduction | $P_{Diode} = V_{Do}I_{Do,Avg} + I^2_{Do,RMS}r_{Do} + V_{Dp}I_{Dp,Avg} + I^2_{Dp,RMS}r_{Dp}$ | |
| Inductor loss | $P_{L,ESR} = \sum_{k=1}^{3} I^2_{Lk,RMS}r_{Lk}$ | |
| Capacitor loss | $P_{C,ESR} = \sum_{k=1}^{2} I^2_{Ck,RMS}r_{Ck}$ | |

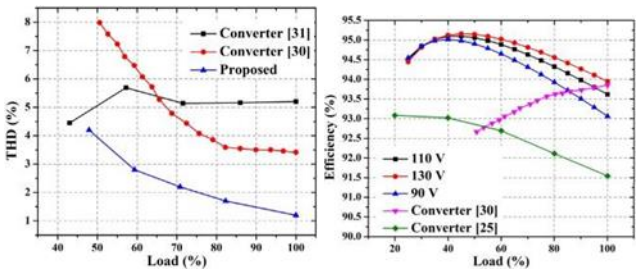


Component count Size and weight Overall system cost

Effective Utilization of Solar PV Energy

The system efficiently extracts and conditions power from the PV panel, supporting sustainable charging for Light Electric Vehicles (LEVs).

Bidirectional/Adaptive Capability (if designed)

Can support varying solar irradiance and load conditions, ensuring consistent performance under dynamic environments.

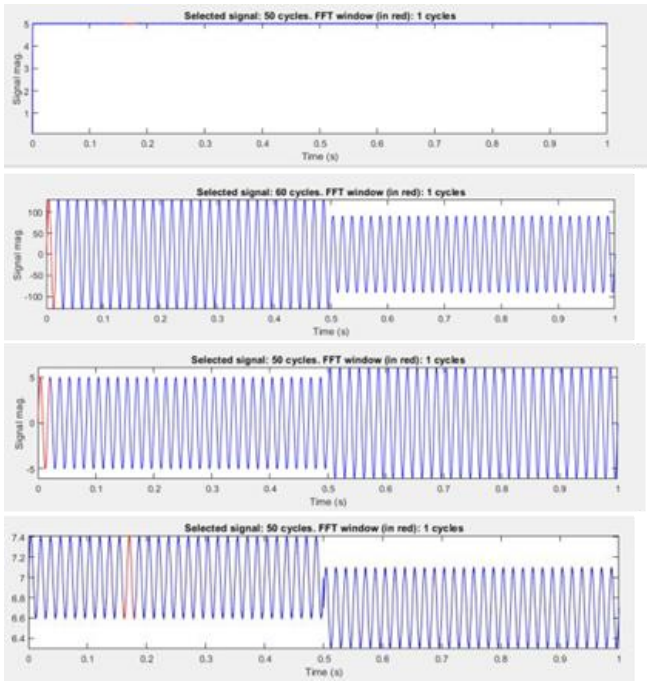


.Voltage sag of Vac

**CONCLUSION**

The simulation results validate the performance and effectiveness of the proposed single-stage PV-based EV charging station interfaced with a three-phase grid. The system successfully integrates a solar PV array, a bidirectional DC-DC converter, and a voltage source converter (VSC) under a unified control strategy. The simulations confirm stable operation in both grid-connected and standalone modes while maintaining DC-link voltage regulation and controlled EV battery charging/discharging. Under steady-state

conditions, the grid currents remain balanced and sinusoidal with total harmonic distortion (THD) maintained within IEEE-519 limits. The power factor remains close to unity, demonstrating effective synchronization and accurate reference current generation. The bidirectional converter enables smooth transition between grid-to-vehicle (G2V) and vehicle-to-grid (V2G) modes without introducing current ripple to the battery. During dynamic conditions such as variations in solar insolation and grid voltage unbalance, the system exhibits strong robustness. Power flow is properly managed between PV, EV battery, and grid without instability. Seamless transition to standalone mode during grid failure and smooth resynchronization upon grid restoration further validate system reliability. Overall, the simulation studies confirm improved power quality, operational flexibility, and suitability for smart grid applications.

## Conflict of interest statement

Authors declare that they do not have any conflict of interest.

## REFERENCES


[1] B. Vardani and N. R. Tummuru, "A single-stage bidirectional inductive power transfer system with closed-loop current control strategy," IEEE Trans. Transport. Electrific., vol. 6, no. 3, pp. 948–957, Sep. 2020.

[2] S. R. Meher and R. K. Singh, "A standard two stage on-board charger with single controlled PWM and minimum switch count," IEEE Trans. Ind. Appl., vol. 59, no. 4, pp. 4628–4639, Jul./Aug. 2023.

[3] A. Singh, J. Gupta, and B. Singh, "Design and control of two stage battery charger for low voltage electric vehicles using high gain buck- boost PFC AC–DC converter," IEEE Trans. Ind. Appl., vol. 59, no. 5,pp. 6125–6135, Sep./Oct. 2023.

[4] M. Tong, M. Cheng, S. Wang, and W. Hua, "An on-board two-stage integrated fast battery charger for EVs based on a five-phase hybrid- excitation flux-switching machine," IEEE Trans. Ind. Electron., vol. 68, no. 2, pp. 1780–1790, Feb. 2021.

[5] C.-Y. Oh, D.-H. Kim, D.-G. Woo, W.-Y. Sung, Y.-S. Kim, and B.-K. Lee,"A high-efficient nonisolated single-stage on-board battery charger for electric vehicles," IEEE Trans. Power Electron., vol. 28, no. 12,pp. 5746–5757, Dec. 2013.

[6] A. V. J. S. Praneeth and S. S. Williamson, "Modeling, design, analysis, and control of a nonisolated universal on-board battery charger for electric transportation," IEEE Trans. Transport. Electrific., vol. 5, no. 4,pp. 912–924, Dec. 2019.

[7] J. Gupta and B. Singh, "A general purpose transformerless charging system based on fully bridgeless canonical switching cell high quality rectifier for LVEVs," IEEE Trans. Transport. Electrific., vol. 9, no. 3,pp. 4211–4222, Sep. 2023.

[8] L. Huber, Y. Jang, and M. M. Jovanovic, "Performance evaluation of bridgeless PFC boost rectifiers," IEEE Trans. Power Electron., vol. 23, no. 3, pp. 1381–1390, May 2008.

[9] A. A. Fardoun, E. H. Ismail, A. J. Sabzali, and M. A. Al-Saffar, "New efficient bridgeless cuk rectifiers for PFC applications," IEEE Trans. Power Electron., vol. 27, no. 7, pp. 3292–3301, Jul. 2012.

[10] S. Singh and B. Singh, "A voltage-controlled PFC Cuk converter-based PMBLDCM drive for air-conditioners," IEEE Trans. Ind. Appl., vol. 48, no. 2, pp. 832–838, Mar. 2012.

[11] V. Bist and B. Singh, "A unity power factor bridgeless isolated Cuk converter-fed brushless DC motor drive," IEEE Trans. Ind. Electron., vol. 62, no. 7, pp. 4118–4129, Jul. 2015.

[12] Y. Liu, Y. Sun, and M. Su, "A control method for bridgeless Cuk/Sepic PFC rectifier to achieve power decoupling," IEEE Trans. Ind. Electron., vol. 64, no. 9, pp. 7272–7276, Sep. 2017.

[13] X. Lin, Z. Jin, F. Wang, and J. Luo, "A novel bridgeless Cuk PFC converter with further reduced conduction losses and simple circuit structure," IEEE Trans. Ind. Electron., vol. 68, no. 11, pp. 10699–10708, Nov. 2021.

[14] A. Shameli, M. Moghsoudi, and H. Farzanehfard, "Bridgeless Cuk PFC converter with soft switching in full input voltage and load range," IEEE Trans. Ind. Electron., early access, Aug. 21, 2023, doi: 10.1109/TIE.2023.3301543.

[15] J. Gupta, R. Kushwaha, and B. Singh, "Improved power quality transformerless single-stage bridgeless converter based charger for light electric vehicles," IEEE Trans. Power Electron., vol. 36, no. 7,pp. 7716–7724, Jul. 2021.

[16] G. Kumar and B. Singh, "Dual-input bridgeless PFC charger for solar photovoltaic panel mounted light electric vehicle," in Proc. IEEE Transp. Electrific. Conf. (ITEC-India), New Delhi, India, Dec. 2021, pp. 1–6.

[17] Y.-C. Hsu, S.-C. Kao, C.-Y. Ho, P.-H. Jhou,M.-Z. Lu, and C.-M. Liaw,"On an electric scooter with G2V/V2H/V2G and energy harvesting functions," IEEE Trans. Power Electron., vol. 33, no. 8, pp. 6910–6925, Aug. 2018.